# The Quasi-Linear Equilibration of a Thermally Maintained, Stochastically Excited Jet in a Quasigeostrophic Model

TIMOTHY DELSOLE

*Data Assimilation Office, NASA/Goddard Space Flight Center, Greenbelt, Maryland*

BRIAN F. FARRELL

*Department of Earth and Planetary Sciences, Harvard University, Cambridge, Massachusetts*

(Manuscript received 25 January 1995, in final form 25 September 1995)

ABSTRACT

A theory for quasigeostrophic turbulence in baroclinic jets is examined in which interaction between the mean flow and the perturbations is explicitly modeled by the nonnormal operator obtained by linearization about the mean flow, while the eddy–eddy interactions are parameterized by a combination of stochastic excitation and effective dissipation. The quasi-linear equilibrium is the stationary state in dynamical balance between the mean flow forcing and eddy forcing produced by the linear stochastic model. The turbulence model depends on two parameters that specify the magnitude of the effective dissipation and stochastic excitation. The quasi-linear model produces heat fluxes (upgradient), momentum fluxes, and mean zonal winds, which are remarkably consistent with those produced by the nonlinear model over a wide range of parameter values despite energy and enstrophy imbalances associated with the parameterization for eddy–eddy interactions. The quasi-linear equilibrium also appears consistent with most aspects of the energy cycle, with baroclinic adjustment (though the adjustment is accomplished in a fundamentally different manner), and with the negative correlation between transient eddy transport and other transports observed in the atmosphere. The model overestimates the equilibrium eddy kinetic energy in cases in which it achieves correct eddy fluxes and energy balance. Understanding the role of forcing orthogonal functions rationalizes this behavior and provides the basis for addressing the role of transient eddies in climate.

## 1. Introduction

Normal mode instability theory, as elucidated by Charney (1947) and Eady (1949), has been widely accepted as a paradigm for understanding the origin of transient eddies dominating atmospheric fluctuations on periods ranging from a few days to weeks. Theoretical difficulties and lack of correspondence with observations of developments on synoptic and planetary scales led to the introduction of nonmodal development theory (Farrell 1982, 1984, 1985, 1989). The normal mode paradigm has led to a variety of climate equilibration theories in which finite amplitude normal modes play a dominant role. For example, Held (1978) and Branscome (1983) have postulated that the mean transient eddy flux is determined in structure by the most unstable normal mode and in magnitude by the mean available potential energy; Stone (1978), Lindzen and Farrell (1980), Gutowski (1985), and Lindzen (1993) have postulated that eddies act to adjust the background state to a configuration that is marginally unstable to normal modes. The nonmodal paradigm has led to stochastic models for eddy variance and fluxes of heat and momentum produced by transient, nonmodal disturbances that are excited randomly in space and time (Farrell and Ioannou 1993, 1994, 1995). In this work, the climate equilibration implied by these stochastically determined fluxes will be obtained.

The equilibration problem for either paradigm may be formulated as follows. Let the nonlinear equations of motion be written in the form

$$\frac{\partial \phi_i}{\partial t} = \mathbf{W}_i(\phi_1, \phi_2, \phi_3, \cdots, \phi_N) = \mathbf{W}_i(\phi), \quad (1)$$

where $\phi_i$ is the $i$th component of an $N$-dimensional state vector. Assuming the existence of a statistically stationary state, the equations can be decomposed into a time-mean component, denoted by a bar, and a deviation therefrom, denoted by a prime. If the equations are at most quadratically nonlinear, as is the case for the Navier–Stokes equations and for the inviscid primitive equations (in Cartesian coordinates), then the equations become

*Corresponding author address:* Tim DelSole, Code 910.3, NASA/Goddard Space Flight Center, Greenbelt, MD 20771.
E-mail: delsole@hera.gsfc.nasa.gov

$$\text{mean} \quad 0 = \mathbf{W}_i(\bar{\phi}) + \frac{1}{2}\left(\frac{\partial^2 \mathbf{W}_i}{\partial\phi_j\partial\phi_k}\right)_{\bar{\phi}} \overline{\phi_j'\phi_k'} \quad (2)$$

$$\text{eddy} \quad \frac{\partial\phi_i'}{\partial t} = \left(\frac{\partial \mathbf{W}_i}{\partial\phi_j}\right)_{\bar{\phi}} \phi_j' + \frac{1}{2}\left(\frac{\partial^2 \mathbf{W}_i}{\partial\phi_j\partial\phi_k}\right)_{\bar{\phi}} (\phi_j'\phi_k' - \overline{\phi_j'\phi_k'}). \quad (3)$$

Equilibration theories address the nontrivial case in which the eddy fluxes balance the mean flow forcing and dissipation $\mathbf{W}_i(\bar{\phi})$. In such cases, the eddy equation (3) is necessarily nonlinear, and the role of eddy nonlinearities must be explicitly addressed. Equilibration theories that do not explicitly include these terms must advance additional hypotheses to uniquely specify the equilibrated state. This is especially true of adjustment theories since the operator

$$\mathbf{L} = \left(\frac{\partial \mathbf{W}_i}{\partial\phi_j}\right)_{\bar{\phi}} \quad (4)$$

can be stable for a large subspace of three-dimensional flow configurations.

Stochastic models explicitly parameterize the nonlinear eddy terms in (3) by an effective dissipation and stochastic excitation. Farrell and Ioannou (1993, 1994, 1995) and DelSole and Farrell (1995) have shown that reasonable heat fluxes, momentum fluxes, and wavenumber/frequency spectra of geopotential height can be obtained from stochastic models in the case in which the operators used to parameterize the nonlinear terms are assumed to be diagonal in the gridpoint representation. These models essentially depend on two parameters, which specify the magnitude of the dissipation and the stochastic excitation due to turbulent eddies. (The models also require specification of the spatial scale below which the stochastic excitation is negligible.) These studies reveal that the stochastic model can be extraordinarily sensitive to changes in the background state when the flow is only slightly stable. The fact that the stochastic model yields realistic eddy fluxes for realistic basic states makes plausible that a critical point $\bar{\phi}$ exists that can satisfy (2) using the eddy fluxes generated by the stochastic model. It remains unclear, however, whether the critical point is stable. The goal of this work is to show that critical points of the coupled equation (2) and the stochastic parameterization of (3) are stable and realistic.

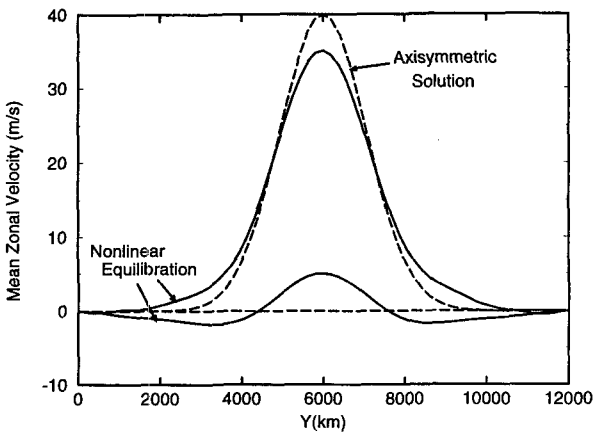


FIG. 1. Mean zonal velocity in the upper and lower layers of the two-layer quasigeostrophic model as a function of meridional location for the axisymmetric solution (dash) and the 1200-day average velocity for the nonlinearly equilibrated flow (solid). The nonlinear equilibrium jet is thermally relaxed toward the axisymmetric solution on a 20-day timescale, and the lower-layer velocities are dissipated on a 5-day timescale. The Phillips criteria for the critical velocity difference for linear instability is 16 m $s^{-1}$.

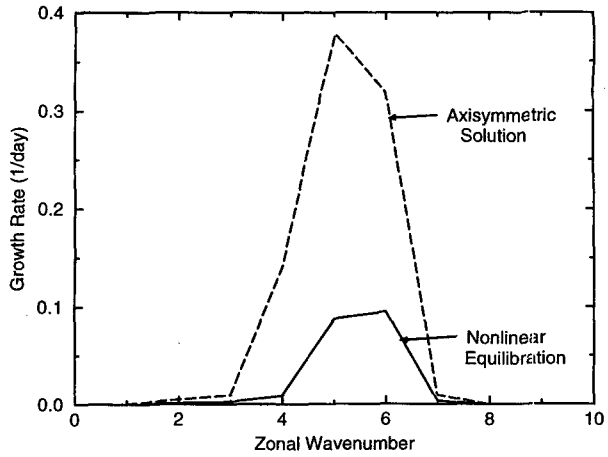


FIG. 2. Growth rates as a function of zonal wavenumber of the most unstable eigenmodes of the linearized equations associated with the axisymmetric solution (dashed) and the 1200-day average velocity (solid) shown in Fig. 1. Both cases include the dissipation due to thermal relaxation and lower-layer friction.

We address this problem using a two-layer quasigeostrophic model that is thermally forced by Newtonian relaxation and dissipated by lower-layer Rayleigh friction. The three-way mean flow balance among the thermal forcing, Rayleigh friction, and the stochastically excited eddy fluxes is called the quasi-linear equilibrium and is obtained by solving (2) and (3) simultaneously for $\bar{\phi}$ (when the nonlinear eddy terms have been parameterized). This procedure is described for the two-layer quasigeostrophic model in section 2. Principle oscillation pattern (POP) analysis is applied in section 3 to a particular nonlinear equilibrium to estimate the unspecified parameters in the stochastic model. Many aspects of the quasi-linear equilibrium are shown in section 4 to be remarkably insensitive to the details of the dissipation and stochastic excitation. The concept of forcing orthogonal functions (FOF's) is discussed in section 5 and, in particular, it is shown that the optimals of Farrell (1989) and the FOF's are mathematically related and that this relation provides a basis for understanding the role of short-lived transient dis-

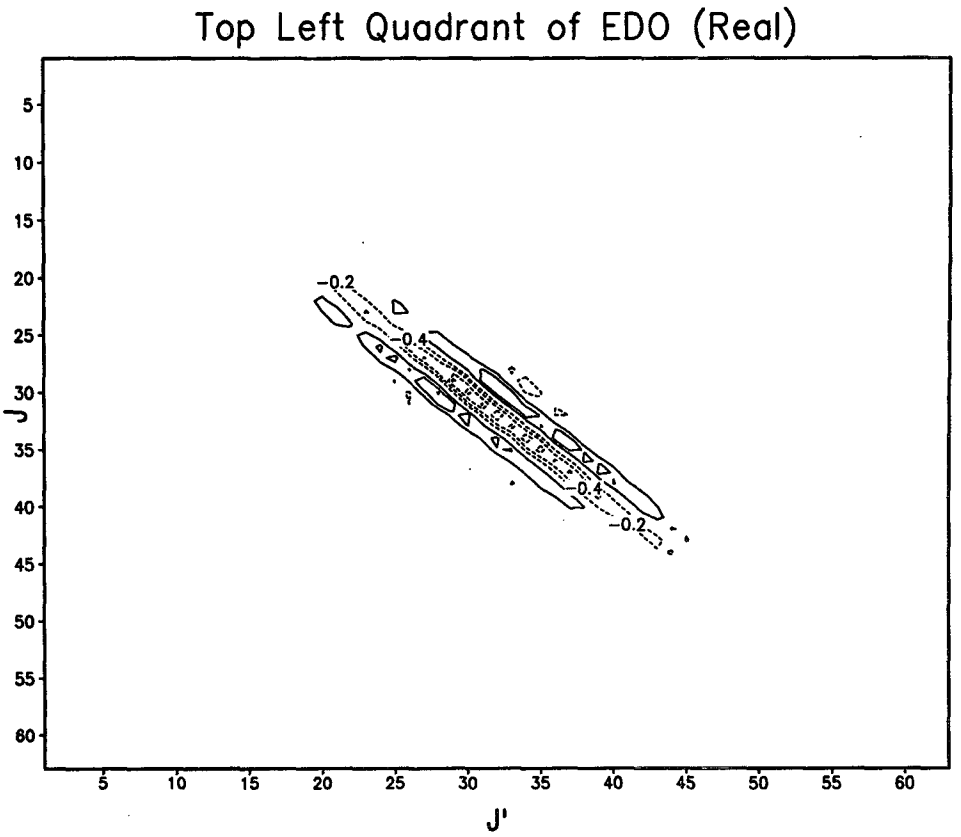


FIG. 3. Real part of the dynamic operator $\mathbf{M} = \mathbf{A}_k - \mathbf{L}_k$, which represents the empirical effective dissipation. The operator $\mathbf{A}_k$ is determined from POP analysis of the 1200-day dataset generated by the nonlinear model for the parameters $k = 6$, $\tau = 0.25$ days. The operator $\mathbf{L}_k$ is the operator associated with the linearized equations of motion (4). The statevector to be multiplied with this operator is composed of 128 elements, the first 64 of which give the gridpoint values of the streamfunction in the upper layer, ordered from south to north, and the last 64 are the values of the streamfunction in the lower layer, again ordered from south to north. Thus, the upper-left quadrant of $\mathbf{M}$ is the dynamic operator giving the tendency of the upper-layer streamfunction due to the instantaneous values of the upper-layer streamfunction. Only the matrix elements $m_{j,j'}$ corresponding to the upper-left quadrant of $\mathbf{M}$ are shown, the elements in the other quadrants were relatively small. The operator clearly exhibits a tridiagonal structure, indicating that the effective dissipation due to nonlinear wave–wave interactions depends on a low-order meridional gradient of the streamfunction.

turbances in the long-term equilibration. Finally, we close by summarizing these results and discussing their implications for understanding transient eddy transport.

## 2. Parameterizing the nonlinear model

We choose a zonally periodic two-layer channel model whose zonally symmetric temperature is relaxed toward an erf function in $y$ (to give a Gaussian baroclinic jet) with a 20-day time constant and whose lower layer is damped by Rayleigh friction with a time constant of 5 days. The equations are split into coupled mean and eddy components (2) and (3) and the nonlinear eddy terms are parameterized by stochastic excitation and effective dissipation. The stochastic excitation consists of independent white noise processes of magnitude $q$ applied to each Fourier zonal and meridional wavenumber pair $(k, l)$. In the stochastic model, the effective dissipation is usually assumed to be Rayleigh friction with magnitude $r_E$ in both layers. A combination of implicit time integration and Newton–Raphson root-finding techniques are employed to find the stationary state that satisfies (2) and (3) simultaneously. What follows is a technical elaboration of this procedure.

The fully nonlinear equations for this model are (cf. Cehelsky and Tung 1987)

$$(\nabla^2\psi)_t + \mathrm{J}(\psi, \nabla^2\psi) + \mathrm{J}(\theta, \nabla^2\theta) + \beta\psi_x = -\mathrm{r_D}\nabla^2(\psi - \theta) \quad (5)$$

$$(\nabla^2\theta - 2\lambda^2\theta)_t + \mathrm{J}(\psi, \nabla^2\theta - 2\lambda^2\theta) + \mathrm{J}(\theta, \nabla^2\psi) + \beta\theta_x = \mathrm{r_D}\nabla^2(\psi - \theta) - 2\lambda^2\mathrm{r_R}(\Theta^* - \theta), \quad (6)$$

where the Jacobian operator is defined to be

$$\mathrm{J}(A, B) = A_xB_y - A_yB_x \quad (7)$$

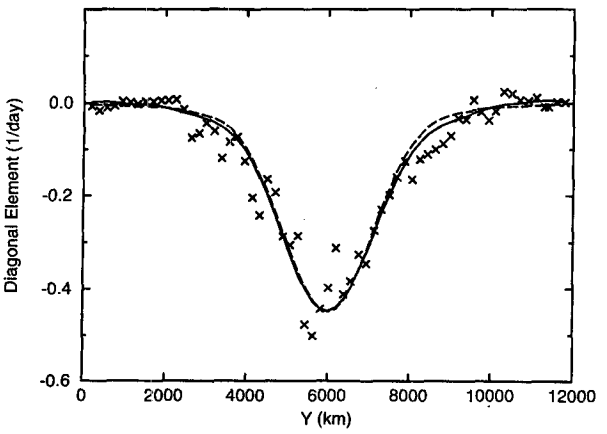


FIG. 4. Diagonal elements ($x$) of the real part of the operator $\mathbf{A}_k - \mathbf{L}_k$ shown in Fig. 3 expressed as a function of meridional distance $y = j\Delta y$, where $\Delta y$ is the distance between grid points in the meridional direction ($j = j'$ in the notation given in Fig. 3). These elements provide a measure of the magnitude of effective dissipation due to nonlinear eddy–eddy interactions. Also shown are the equilibrated upper-layer zonal velocity (solid) and the upper-layer eddy streamfunction variance associated with zonal wavenumber 6 (dash), both scaled and sign reversed to fit on the graph. The similarity in profiles suggests that the effective dissipation is related to the local eddy variance/mean zonal velocity.

and the barotropic and baroclinic streamfunctions are given by

$$\psi = \frac{\psi_{\text{upper}} + \psi_{\text{lower}}}{2} \quad \theta = \frac{\psi_{\text{upper}} - \psi_{\text{lower}}}{2}. \tag{8}$$

The boundary conditions are periodicity in the zonal direction, $x$, and rigid, free-slip walls at $y = 0$ and $y = L_y$. The parameter $r_D$ is the lower-layer frictional damping rate, $r_R$ is the thermal damping rate, $1/\lambda$ is the Rossby radius, and $\Theta^*$ is proportional to the radiative-equilibrium temperature.

Consider the nonlinear system initialized arbitrarily and allowed to evolve for a sufficiently long time to ensure stationary statistics. Anticipating that the time-mean state is zonally symmetric, "eddy" refers to deviations from both time and zonal mean. To model the system with a stochastic turbulence parameterization, we first separate the equations into eddy and mean components. Using an overbar and/or uppercase letters to refer to zonal mean quantities and lowercase letters to refer to eddy quantities, we first write (5)–(6) in their zonally averaged form:

$$\Psi_{yyt} + (\overline{\psi_x\psi_{yy} + \theta_x\theta_{yy}})_y = -r_D(\Psi_{yy} - \Theta_{yy}) \tag{9}$$

$$(\Theta_{yy} - 2\lambda^2\Theta)_t + (\overline{\psi_x\theta_{yy} + \theta_x\psi_{yy} - 2\lambda^2\psi_x\theta})_y = -r_D(\Theta_{yy} - \Psi_{yy}) - 2\lambda^2 r_R(\Theta^* - \Theta) \tag{10}$$

and then subtract these from (5)–(6) to obtain the equations governing the zonal deviations

$$\nabla^2\psi_t + U(\nabla^2\psi)_x + H(\nabla^2\theta)_x + (\beta - U_{yy})\psi_x - H_{yy}\theta_x = -r_D\nabla^2(\psi - \theta) - J(\psi, \nabla^2\psi)' - J(\theta, \nabla^2\theta)' \tag{11}$$

$$(\nabla^2\theta - 2\lambda^2\theta)_t + U(\nabla^2\theta)_x + H(\nabla^2\psi)_x - 2\lambda^2 U\theta_x + 2\lambda^2 H\psi_x + (\beta - U_{yy})\theta_x - H_{yy}\psi_x = -r_D\nabla^2(\theta - \psi) + 2\lambda^2 r_R\theta + 2\lambda^2 J(\psi, \theta)' - J(\psi, \nabla^2\theta)' - J(\theta, \nabla^2\psi)', \tag{12}$$

where $U = -\Psi_y$ and $H = -\Theta_y$. The prime Jacobian terms refer to the nonlinear eddy components of the Jacobian,

$$J(A, B)' = J(A', B') - \overline{J(A', B')}. \tag{13}$$

The nonlinear eddy terms are parameterized by an effective dissipation and stochastic excitation. For a variety of reasons that should become clear later, the parameters will be constrained to be representable by diagonal operators in the Fourier representation. Moreover, the parameters associated with sufficiently small scales are assumed negligible. To be specific, the stochastic excitation is chosen so that the first 8 zonal wavenumbers and the first 40 meridional wavenumbers are forced equally and independently. In many cases the excitation of the meridional wavenumbers will be weighted by $g_l$ to be consistent with the meridional structure found from POP analysis discussed in section 3, but each wavenumber will still be forced independently. In either case the stochastic excitation depends on one parameter, denoted by $q$, that can be related to the total energy injection by the stochastic excitation. The effective dissipation is assumed to be either Rayleigh friction with magnitude $r_E$ or second-order diffusion of potential vorticity with magnitude $\nu$. For an individual experiment, the full parameterization depends on just two parameters, $r_E$ and $q$, that determine the stochastic excitation and effective dissipation. Specifically, the nonlinear terms in (11) and (12) are parameterized as follows:

$$-J(\psi, \nabla^2\psi)' - J(\theta, \nabla^2\theta)' = q\sum_{k=1}^{8}\sum_{l=1}^{40} g_l \,\mathrm{Re}[\epsilon_\psi^{k,l}(t)e^{ikx}\sin(ly)] - r_E\nabla^2\psi \tag{14}$$

$$J(\psi, 2\lambda^2\theta)' - J(\psi, \nabla^2\theta)' - J(\theta, \nabla^2\psi)' = q\sum_{k=1}^{8}\sum_{l=1}^{40} g_l \,\mathrm{Re}[\epsilon_\theta^{k,l}(t)e^{ikx}\sin(ly)] - r_E\nabla^2\theta. \tag{15}$$

The stochastic excitation functions $\epsilon_\psi^{k,l}$, $\epsilon_\theta^{k,l}$ have the properties

$$\langle\epsilon_\psi^{k,l}(t)[\epsilon_\psi^{k',l'}(t')]^*\rangle = \delta(t - t')\delta_{k,k'}\delta_{l,l'} \tag{16}$$

$$\langle\epsilon_\theta^{k,l}(t)[\epsilon_\theta^{k',l'}(t')]^*\rangle = \delta(t - t')\delta_{k,k'}\delta_{l,l'} \tag{17}$$

$$\langle\epsilon_\theta^{k,l}(t)[\epsilon_\psi^{k',l'}(t')]^*\rangle = 0, \tag{18}$$

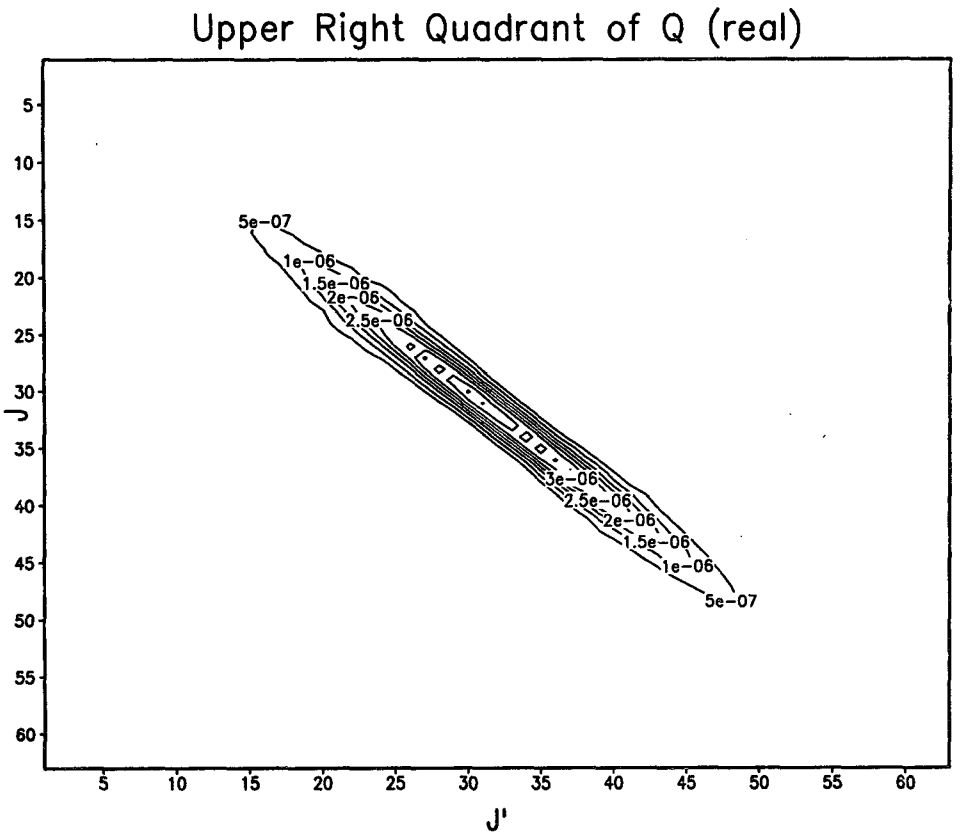


FIG. 5. Real part of the forcing covariance matrix $\mathbf{Q}_k$ determined from POP analysis using the 1200-day dataset generated by the nonlinear model using the parameters $\tau = 0.25$ days and $k = 6$. The format of the operator is the same as that of $\mathbf{A}_k - \mathbf{L}_k$ shown in Fig. 3—the upper left quadrant gives covariance matrix of the stochastic excitation applied to the upper layer, zonal wavenumber 6 streamfunction at each meridional grid point. The matrix elements in the other quadrants are much smaller. The units are $km^4\ s^{-3}$. The result indicates that the stochastic excitation for this streamfunction is meridionally localized.

where the angle brackets $\langle\ \rangle$ denote ensemble averages, asterisks denote the complex conjugate, $\delta(t - t')$ denotes the Dirac delta function, and $\delta_{k,k'}$ denotes the Kronecker delta which is unity when $k = k'$ and vanishes otherwise. The resulting parameterization of (11) and (12) yields

$$\nabla^2\psi_t + \mathrm{U}(\nabla^2\psi)_x + \mathrm{H}(\nabla^2\theta)_x + (\beta - \mathrm{U}_{yy})\psi_x - \mathrm{H}_{yy}\theta_x = -\mathrm{r_D}\nabla^2(\psi - \theta) - \mathrm{r_E}\nabla^2\psi + q\sum_{k=1}^{8}\sum_{l=1}^{40} g_l\,\mathrm{Re}[\epsilon_\psi^{k,l}(t)e^{ikx}\sin(ly)] \quad (19)$$

$$(\nabla^2\theta - 2\lambda^2\theta)_t + \mathrm{U}(\nabla^2\theta - 2\lambda^2\theta)_x + 2\lambda^2\mathrm{H}\psi_x + \mathrm{H}(\nabla^2\psi)_x + (\beta - \mathrm{U}_{yy})\theta_x - \mathrm{H}_{yy}\psi_x = -\mathrm{r_D}\nabla^2(\theta - \psi) - \mathrm{r_E}\nabla^2\theta + 2\lambda^2\mathrm{r_R}\theta + q\sum_{k=1}^{8}\sum_{l=1}^{40} g_l\,\mathrm{Re}[\epsilon_\theta^{k,l}(t)e^{ikx}\sin(ly)]. \quad (20)$$

Equations (19) and (20) are stochastically excited linear equations that can be solved by the methods discussed in appendix A. Explicit solutions are most easily obtained using a spectral technique, which is discussed in appendix B. Having specified the magnitude of effective dissipation and stochastic excitation through $q$, $\mathrm{r_E}$, only the zonal mean velocities $\mathrm{U}(y)$ and $\mathrm{H}(y)$ remain undetermined. We adopt the following iterative method to find this equilibrium solution. For fixed $\mathrm{r_E}$ and $q$, the eddy covariances resulting from the stochastic differential equations (19)–(20) are substituted for the nonlinear eddy terms in (9)–(10) to obtain the tendency of the mean flow. The zonal mean velocities $\mathrm{U}(y)$ and $\mathrm{H}(y)$ are advanced to the next time step and used in the linear, stochastic differential equations (19)–(20) to update the eddy fluxes. These calculations are repeated until the time derivatives of the zonal mean velocities U and H in (9)–(10) are sufficiently small that convergence is indicated (a practical method requires semi-implicit integration as discussed in appendix C). The final solution is the quasi-linear equilibrated jet. Two distinct timescales are involved in this iteration: these are the time step used to advance the zonal-mean velocities in (9)–(10), which is on the order of an hour, and the time required for the sto-

TABLE 1. Quasi-linear equilibration under different dissipations.

| Rayleigh uniform ($d^{-1}$) | Rayleigh $y$-dep. ($d^{-1}$) | Diffusion uniform ($km^2\ s^{-1}$) | Diffusion $y$-dep. ($km^2\ s^{-1}$) | $\omega_{r,max}$ ($d^{-1}$) | $k_{max}$ | Type of jet* | Figure |
|---|---|---|---|---|---|---|---|
| 2.00 | 0 | 0 | 0 | −0.1320 | 1 | A (Wide) | — |
| 0.20 | 0 | 0 | 0 | −0.0192 | 5 | A | Fig. 6 |
| 0.02 | 0 | 0 | 0 | −0.0018 | 6 | $B^{EW}$ | — |
| 0 | 2.00 | 0 | 0 | −0.0028 | 8 | $B^{EW,3}$ | — |
| 0 | 0.20 | 0 | 0 | −0.0063 | 8 | C | — |
| 0 | 0.02 | 0 | 0 | −0.0008 | 6 | B (Wide) | — |
| 0 | 0 | 0.4 | 0 | −0.0167 | 5 | B | Fig. 7 |
| 0 | 0 | 4.0 | 0 | −0.0888 | 1 | A | Fig. 7 |
| 0 | 0 | 40.0 | 0 | −0.0327 | 1 | A | Fig. 7 |
| 0 | 0 | 0 | 0.04 | −0.0012 | 6 | $B^{EW}$ | — |
| 0 | 0 | 0 | 0.40 | −0.0057 | 5 | B | — |
| 0 | 0 | 0 | 4.00 | −0.0310 | 8 | A (Wide) | — |
| 0 | 0 | 0 | 40.00 | −0.0301 | 6 | B (Wide) | — |

* The jets were categorized by the number of westerly extremums: type A has 1 extremum and is close to Gaussian, type B has three extrema with the absolute maximum in the channel center, and type C has 2 maximums near the channel walls and 1 minimum in the channel center. Here, "$()^{EW}$" means type ( ) plus two strong easterly jets near each channel wall; and "$B^3$" means all three extremums were comparable in magnitude. "Wide" means the central jet was much broader than the radiative equilibrium thermal wind.

chastically forced linear equations (19)–(20) to obtain their ensemble averages from the previous state, which can be from a day to a few months. These timescales interact to affect the details of the trajectory of the system as it approaches its stationary state but do not affect the stationary state itself. Since we are only interested in determining the stationary state, the variation of this trajectory with the timescales is inconsequential. The time marching scheme should be viewed as a device for finding the stationary state, and the resulting trajectory does not necessarily represent the actual trajectory a nonlinear model would take toward the stationary state.

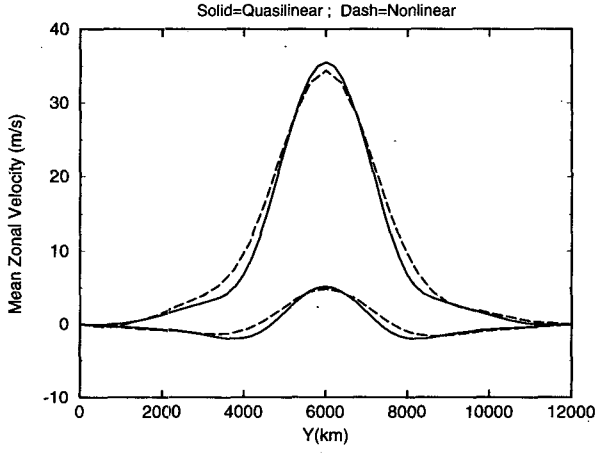


FIG. 6. Upper- and lower-layer mean zonal velocity of the nonlinear equilibrium jet (dash) and the quasi-linear equilibrium jet (solid) with 5-day Rayleigh friction modeling the effective dissipation and temporal white noise forcing with total injection rate of 1.85 W $m^{-2}$ modeling the stochastic excitation. The Rayleigh friction is uniform in both layers; the excitation has the fixed meridional profile shown in Fig. 4 for the eddy streamfunction variance (dash line in Fig. 4) and is the same magnitude in both layers.

The thermally forced flow is chosen to be symmetric about the midchannel so that the mean flow is anticipated to be composed solely of odd meridional wavenumbers and the even and odd wavenumber perturbation components are decoupled. Furthermore, even components are incapable of extracting energy from the symmetric jet and are therefore neglected.

The linear equations are stochastically excited such that the total input energy is 1.85 W $m^{-2}$, a choice motivated by POP analysis to be discussed next. This average rate is also a reasonable value based on the observational evidence (as discussed in DelSole and Farrell 1995). We minimize the dynamical influence of the walls by choosing a relatively large domain (12 000 km) and a zonally symmetric radiative-equilibrium temperature gradient localized in the center of the channel. In particular, the radiative-equilibrium thermal wind is chosen to have a Gaussian profile:

$$-\Theta_y^* = H_0 \exp\left(-\frac{(y - L_Y/2)^2}{b^2}\right), \qquad (21)$$

where $b = 1500$ km and $H_0 = 20$ m $s^{-1}$. The remaining external parameters are chosen for midlatitude zonal mean states. Altogether,

$$L_x = 30\,000 \text{ km} \quad r_R = 0.05\ d^{-1}$$

$$\beta = 1.6 \cdot 10^{-8}\ km^{-1}\ s^{-1}$$

$$L_y = 12\,000 \text{ km} \quad r_D = 0.2\ d^{-1} \quad \lambda = 10^{-3}\ km^{-1}.$$

## 3. POP analysis of nonlinear equilibration

We first integrate the fully nonlinear model (5)–(6) for 1400 days using an energy and enstrophy conserving advection scheme (Arakawa 1966) and a third-order Adams–Bashforth time integration scheme (Durran 1991). The zonal direction is discretized with 32

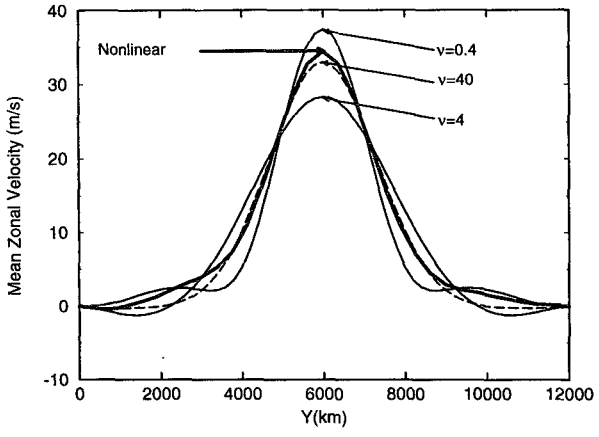


FIG. 7. Upper-layer mean zonal velocity of the quasi-linear solution for four different choices of spatially uniform diffusion coefficient representing the effective dissipation. These profiles should be compared to the nonlinearly equilibrated upper-layer velocity shown in Fig. 1. The stochastic excitation is assumed to have the same meridional profile shown in Fig. 4 for the eddy streamfunction variance and injects 1.85 W $m^{-2}$. The units of diffusion coefficient are $km^2\ s^{-1}$. For comparison, the diffusion coefficient implied by dissipation shown in Fig. 3 is around 0.4 $km^2\ s^{-1}$.

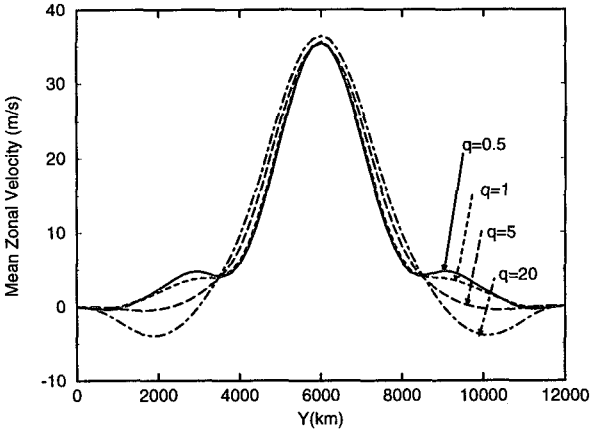


FIG. 8. Upper-layer mean zonal velocity of the quasi-linear equilibrium jet for four different magnitudes of white noise stochastic excitation. These profiles should be compared to the nonlinearly equilibrated upper-layer velocity shown in Fig. 1. Both the stochastic excitation and the diffusion coefficient are assumed to have the same meridional profile shown in Fig. 4 for the eddy streamfunction variance (dash line) and are of the same magnitude in both layers. The units of white noise are in W $m^{-2}$ total injection rate. Note that the excitation changes by a factor of 40, while the upper-layer velocities in the midchannel change by 5%.

points, the meridional direction with 64 points. The resulting mean zonal flow is shown in Fig. 1. A routine eigenanalysis of this flow reveals that zonal wavenumbers 5 and 6 have comparable growth rates (Fig. 2).

Principal oscillation pattern analysis is a procedure for processing a multivariate time series (from whatever source) to empirically determine the first-order Markov model producing the same second-order moments (Penland 1989; von Storch et al. 1995). Under zonally symmetric forcing and boundary conditions, the statistically steady eddy covariances between quantities of differing zonal wavenumber will vanish. It follows that the Markov model governing the statevector $\phi_k$ associated with the $k$th zonal wavenumber will be explicitly uncoupled from the statevector associated with a different zonal wavenumber. There will exist an implicit coupling, however, in that the dynamic operator and stochastic excitation must correctly model the eddy–eddy interactions between all zonal wavenumbers. Remarkably, POP analysis allows the dynamic operator for each zonal wavenumber to be estimated independently of the other zonal wavenumbers. Let $\phi_k$ be a vector whose elements are the meridional gridpoint values of the two-layer streamfunction associated with the $k$th zonal wavenumber. Moreover, let the elements be ordered so that the first 64 elements correspond to the upper-layer meridional gridpoint values from south to north, while the second 64 elements correspond to those for the lower layer. The Markov model for each zonal wavenumber has the form

$$\frac{\partial \phi_k}{\partial t} = \mathbf{A}_k \phi_k + \zeta_k(t), \tag{22}$$

where the forcing term $\zeta_k$ is white noise with forcing covariance matrix $\mathbf{Q}_k$:

$$\frac{1}{T}\int_0^T \zeta_k(t+\tau)\zeta_{k'}^{\mathrm{H}}(t)dt = \mathbf{Q}_k \delta(\tau)\delta_{k,k'}. \tag{23}$$

TABLE 2. Quasi-linear equilibration under different forcing.

| Injection rate (W $m^{-2}$) | Meridional structure | Vertical structure | $\omega_{max}$ ($d^{-1}$) | $k_{max}$ | Type of jet | Figure |
|---|---|---|---|---|---|---|
| 0.5 | standard | barotropic | −0.0040 | 5 | B | Fig. 8 |
| 1.0 | standard | barotropic | −0.0087 | 5 | B | Fig. 8 |
| 5.0 | standard | barotropic | −0.0628 | 6 | A | Fig. 8 |
| 20.0 | standard | barotropic | −0.0729 | 1 | $A^{EW}$ | Fig. 8 |
| 5.0 | standard | upper only | −0.0471 | 5 | A | — |
| 5.0 | standard | lower only | −0.0703 | 1 | B | — |
| 5.0 | uniform | barotropic | −0.0580 | 5 | A | — |
| 5.0 | sin(1) | barotropic | −0.0546 | 6 | $A^{EW}$ | — |
| 5.0 | sin(1 + 3) | barotropic | −0.0661 | 5 | A | — |

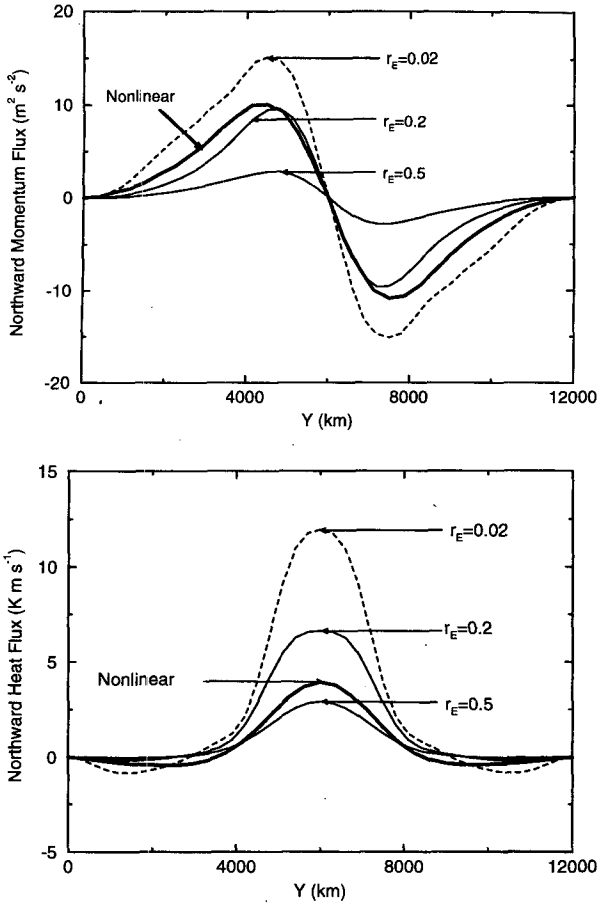


FIG. 9. Vertically averaged, northward momentum flux (a) and heat flux (b) obtained from the nonlinear model and from the stochastic model for four different magnitudes of Rayleigh friction representing the effective dissipation. Note that all profiles correspond to upgradient momentum transfer. The Rayleigh friction is uniform in both layers and is in units of days$^{-1}$. The stochastic excitation, which injects 1.85 W m$^{-2}$ into zonal wavenumbers 1–8 and odd meridional wavenumbers 1–19, has the same magnitude in both layers and has the fixed meridional profile shown in Fig. 4 for the eddy streamfunction variance (dashed line in Fig. 4).

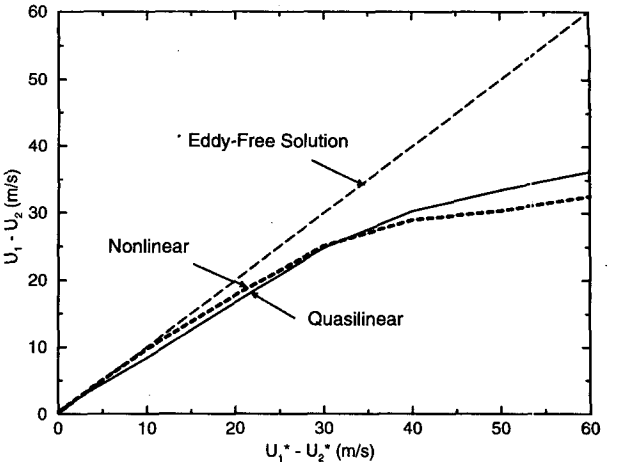


FIG. 10. Equilibrated zonal mean zonal velocity difference between the upper and lower layer at the center of the channel as a function of the forcing of this difference by the thermal relaxation. The parameters used in the quasi-linear model are the same parameters as those used to generate Fig. 6.

The superscript H denotes the conjugate transpose. Note that the forcing is allowed to be spatially correlated since $\mathbf{Q}_k$ is not restricted to be diagonal.

The mean response is represented by the statevector's time-lagged covariance matrix

$$\mathbf{C}_k(\tau) = \frac{1}{T}\int_0^T \phi_k(t+\tau)\phi_k^{\mathrm{H}}(t)dt, \qquad (24)$$

which is estimated from data using the last 1200 days of the 1400-day dataset. It can be shown for a model of the form (22) that this covariance matrix should satisfy the equalities

$$\mathbf{C}_k(\tau) = \exp(\mathbf{A}_k\tau)\mathbf{C}_k(0) \qquad (25)$$

$$\mathbf{A}_k\mathbf{C}_k + \mathbf{C}_k\mathbf{A}_k^{\mathrm{H}} = -\mathbf{Q}_k. \qquad (26)$$

The stochastic model (19) and (20) must satisfy additional requirements to be completely consistent with the data, but these requirements will not be insisted upon since our purpose is to construct the best empirical stochastic model within the confines of (22) and (23). A detailed discussion of these issues and the full procedure can be found in DelSole (1996). The effective dissipation operator is obtained from the real part of $\mathbf{A}_k - \mathbf{L}_k$ [where $\mathbf{L}_k$ is (4)], the top left quadrant of which is shown in Fig. 3 for $k = 6$ (the elements in the other quadrants were small). Although the interpretation of this result is subtle due to data filtering, the result

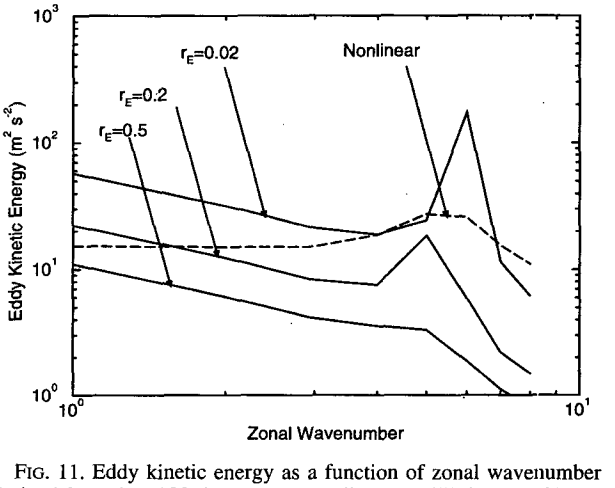


FIG. 11. Eddy kinetic energy as a function of zonal wavenumber derived from the 1200-day average nonlinear equilibrium (dash) and the quasi-linear equilibrium (solids) for three different magnitudes of Rayleigh friction representing effective dissipation. The units of dissipation are per day. The equilibrium jet represented in Fig. 6 corresponds to damping rate 0.2 d$^{-1}$, and the spatial structure of the effective dissipation and stochastic excitation are unchanged between the two cases.

TABLE 3a. Quasi-linear eddy energetics.

| $k$ | C(KM→E) W m$^{-2}$ | C(PM→E) W m$^{-2}$ | GE W m$^{-2}$ | DE W m$^{-2}$ | DE-EFF W m$^{-2}$ | SE W m$^{-2}$ |
|---|---|---|---|---|---|---|
| 1 | 0.027 | 0.029 | −0.051 | −0.224 | −0.525 | 0.744 |
| 2 | 0.020 | 0.031 | −0.036 | −0.109 | −0.291 | 0.385 |
| 3 | 0.005 | 0.048 | −0.027 | −0.062 | −0.195 | 0.231 |
| 4 | −0.032 | 0.120 | −0.026 | −0.041 | −0.178 | 0.157 |
| 5 | −0.232 | 0.662 | −0.052 | −0.059 | −0.435 | 0.115 |
| 6 | −0.077 | 0.171 | −0.008 | −0.036 | −0.140 | 0.089 |
| 7 | −0.021 | 0.024 | −0.002 | −0.019 | −0.052 | 0.071 |
| 8 | −0.013 | 0.007 | −0.001 | −0.014 | −0.035 | 0.057 |
| Total | −0.322 | 1.092 | −0.203 | −0.564 | −1.852 | 1.850 |

suggests that the dissipation depends on a low-order meridional gradient of the streamfunction. Moreover, a strong correlation exists between the diagonal elements and the local velocity and eddy variance (see Fig. 4). Based on these empirical results of POP analysis, we assume that the effective dissipation is Rayleigh friction and/or second-order diffusion for all zonal wavenumbers and for all parameter regimes examined in this work.

The real part of the forcing covariance matrix, $\mathbf{Q}_k$ for $k = 6$, is shown in Fig. 5. As found by DelSole (1996), the forcing also appears to be localized in the meridional direction. Furthermore, a plot of the real diagonal elements of $\mathbf{Q}_k$ with the local mean velocity and eddy variance (not shown) suggests that the forcing also tends to be correlated with the local zonal velocity and eddy variance. The energy injected into zonal wavenumber 6 by this forcing is determined by

$$\frac{\Delta P}{g}\frac{\text{Trace}(\mathbf{B}_k\mathbf{Q}_k)}{2N} = 0.1 \text{ W m}^{-2}, \qquad (27)$$

where $\Delta P/g$ is mass per horizontal area of the atmosphere, $\mathbf{B}_k$ is the potential vorticity operator corresponding to zonal wavenumber 4, and $N$ is the dimension of the model (see appendix A). The sum of the forcing for zonal waves 1–8 is found to be about 2 W m$^{-2}$. It will turn out that choosing $q$ so as to give a total energy injection rate of 1.85 W m$^{-2}$ yields a consistent eddy energy budget (discussed in section 5).

## 4. Quasi-linear equilibration

In this section we examine the quasi-linear equilibrated flow under a few choices for the effective dissipation and stochastic excitation suggested by the POP analysis of the previous section. A few representative examples are summarized in Table 1 and illustrated in Figs. 6–8. By "$y$-dep." we mean that the dissipation has the meridional structure derived from the POP analysis of the nonlinear equilibrium shown in Fig. 4; "uniform" denotes a dissipation that is constant in space and time. The forcing is maintained at 1.85 W m$^{-2}$ in these examples with the meridional structure illustrated in Fig. 4. The quasi-linear equilibrium for $r_E = 0.2$ d$^{-1}$ is illustrated in Fig. 6, which shows that the quasi-linear model gives a good approximation to the nonlinear equilibrium. Essentially, the same jet is obtained for $r_E$ between 0.1 and 0.5 d$^{-1}$. As Rayleigh friction increases from its nominal value of $r_E = 0.2$ d$^{-1}$, the primary change in equilibrated state is a reduction of lower-layer velocities; as the friction decreases from $r_E = 0.2$ d$^{-1}$, the primary change is the appearance of weak secondary jets along the flanks of the primary jet.

Consider the quasi-linear equilibrated jet in the case of $y$-dependent diffusion, illustrated in Fig. 7 over three orders of magnitude for the diffusion coefficient. Results from the POP analysis immediately suggests that the effective dissipation is second-order diffusion with magnitudes from 0.03 to 0.3 km$^2$ s$^{-1}$. It is clear from comparing Fig. 7 to Fig. 1 that this range does indeed yield an equilibrated upper-layer flow very similar to the nonlinearly equilibrated flow. Adding uniform Rayleigh friction of $r_D = 0.05$ d$^{-1}$ renders the equilibrated jet virtually indistinguishable from the nonlinearly equilibrated jet for diffusion coefficients between 0.03 and 0.3 km$^2$ s$^{-1}$. The case of Rayleigh friction maximizing in the midchannel was found to fail in simulating the nonlinearly equilibrated jet except when extremely small values of Rayleigh friction were used (max values 0.002 d$^{-1}$). The difficulty is that using Rayleigh friction that maximizes in the center of the flow damps the eddies in the center, causing the eddies and the associated fluxes to concentrate near the walls.

TABLE 3b. Nonlinear eddy energetics.

| $k$ | C(KM→E) W m$^{-2}$ | C(PM→E) W m$^{-2}$ | GE W m$^{-2}$ | DE W m$^{-2}$ | Transfer W m$^{-2}$ |
|---|---|---|---|---|---|
| 1 | −0.015 | 0.006 | −0.026 | −0.042 | 0.076 |
| 2 | −0.016 | 0.019 | −0.026 | −0.036 | 0.059 |
| 3 | −0.012 | 0.037 | −0.026 | −0.035 | 0.036 |
| 4 | −0.004 | 0.078 | −0.034 | −0.038 | −0.003 |
| 5 | −0.125 | 0.380 | −0.062 | −0.052 | −0.141 |
| 6 | −0.143 | 0.409 | −0.043 | −0.051 | −0.172 |
| 7 | −0.051 | 0.171 | −0.026 | −0.029 | −0.064 |
| 8 | −0.024 | 0.054 | −0.017 | −0.014 | 0.001 |
| Total | −0.390 | 1.154 | −0.260 | −0.297 | −0.208 |

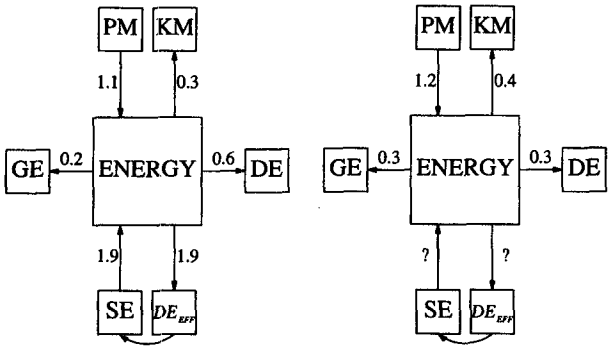


FIG. 12. Total energy budget for zonal wavenumber 1–8 associated with the quasi-linear (left) and nonlinear (right) statistically stationary state shown in Fig. 6. Here, PM denotes the mean potential energy, KM denotes the mean kinetic energy, GE denotes the generation of energy due to thermal relaxation, DE denotes the dissipation of energy due to lower-layer friction, and SE and $DE_{EFF}$ denote the stochastic excitation and effective dissipation, respectively, due to nonlinear eddy interactions. All numbers associated with the arrows are in units of W m$^{-2}$. Note that the stochastically excited eddies extract energy from the available potential energy and inject energy into the mean kinetic energy. The magnitude of the equal but opposite transfers SE and $DE_{eff}$ are indeterminate from observations.

Next, we fixed the Rayleigh friction and varied the stochastic excitation. A representative collection of our results is given in Table 2 and shown in Fig. 8. The quasi-linear equilibrium approximates the nonlinear solution as long as the excitation is applied to the upper layer and has magnitudes in the range 2–10 W m$^{-2}$. This indicates that the quasi-linear equilibrium is largely independent of the details of the excitation when the latter is "reasonable," that is, when the excitation is largest where the eddy variance is largest. Note that the excitation has changed by a factor of 40 yet the equilibrated flow shown in Fig. 8 has changed relatively little. This implies that the underlying eddy fluxes have also changed relatively little. This is in sharp contrast to the purely linear results discussed in Farrell and Ioannou (1994) and DelSole and Farrell (1995) in which the fluxes are directly proportional to the excitation magnitude. The reduction in sensitivity is due to the nonlinear feedback with the background state—because the flow is nearly neutral (with the inclusion of effective dissipation), small changes in the equilibrated state lead to significant changes in the linear response to stochastic excitation. The equilibration near neutral basic states (in which the definition of neutrality includes the effective dissipation) thus allows the equilibrated flow to maintain its basic structure even when the stochastic excitation increases dramatically.

The momentum and heat fluxes for different choices of Rayleigh friction are shown in Figs. 9a,b. First note that all choices lead to upgradient momentum fluxes, in agreement with the nonlinear mean fluxes. Second, comparison with the nonlinear results suggest that the correct magnitude of dissipation is 1–5 d$^{-1}$. The same conclusion holds for heat fluxes. It thus appears that the quasi-linear system models the nonlinear equilibration in a consistent manner.

## 5. Further aspects of the equilibration

The quasi-linear model is consistent with baroclinic adjustment in the sense that as the thermal gradient is varied, the heat flux increases abruptly when the gradient exceeds a critical value. The result of such eddy behavior is to yield an equilibrated flow near this crit-

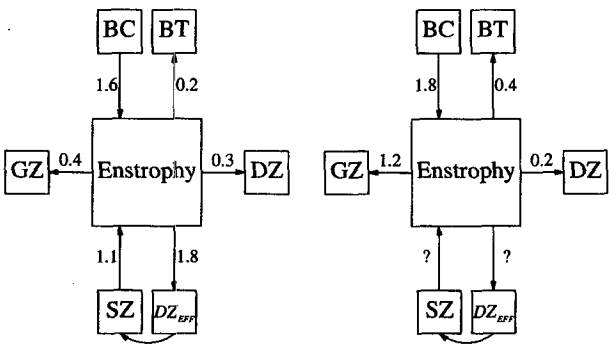


FIG. 13. Total enstrophy budget for zonal wavenumbers 1–8 associated with the quasi-linear (left) and nonlinear (right) statistically steady states shown in Fig. 6. All numbers are in units of 0.1 day$^{-3}$. The symbols in boxes are explicitly defined in the text and are analogous to the terms found in the energy budget equations. The magnitude of the equal but opposite transfers SZ and $DZ_{eff}$ and indeterminate from observations.

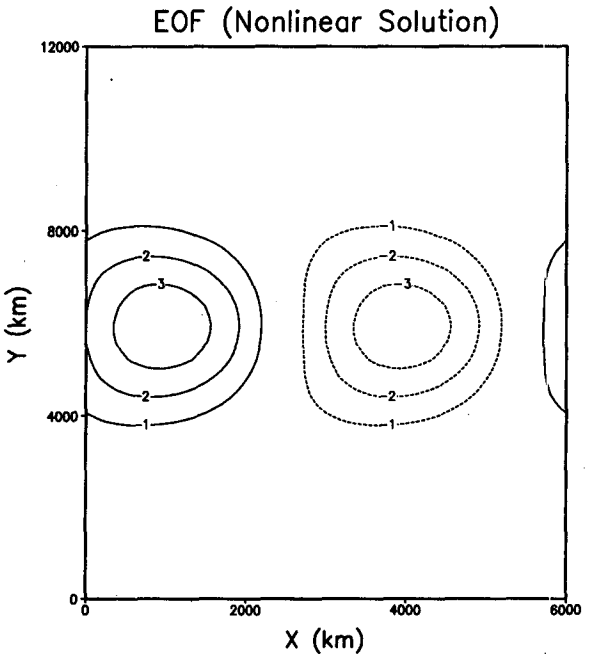


FIG. 14. First, upper-layer streamfunction EOF associated with the *nonlinear* equilibration shown in Fig. 6. The figure shows only a portion of the channel corresponding to one zonal wavelength of wavenumber 5. The zonal phase and amplitude are arbitrary.

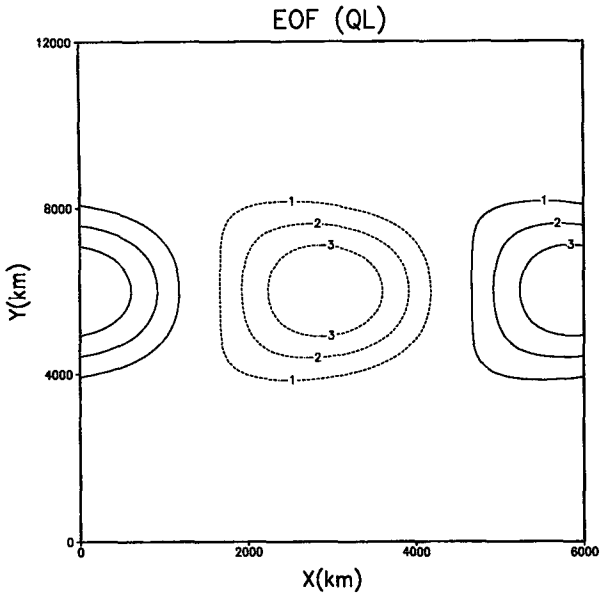


FIG. 15. Upper-layer streamfunction EOF associated with the *quasi-linear* equilibration shown in Fig. 6. This EOF is to be compared with the corresponding EOF derived from the nonlinear solution shown in Fig. 14. The figure shows only a portion of the channel corresponding to one zonal wavelength of wavenumber 5. The zonal phase and amplitude are arbitrary.

ical gradient that is robust against increases in thermal forcing (Stone 1978; Held 1978). This behavior is shown to occur in Fig. 10 in which the zonal time-mean vertical shear $U_{upper} - U_{lower}$ at the center of the channel, which is proportional to the temperature gradient at the center of the channel, is used to measure the mean-flow adjustment. Remarkably, the quasi-linear equilibrium approximates the nonlinear solution with constant turbulence parameters $q$ and $r_E$. The reason the quasi-linear model produces robust equilibrations at strong thermal forcing is that stochastic models tend toward unbounded responses as the state is driven toward neutrality. In nearly neutral states, small adjustments in the basic state induce large changes in the eddy response of stochastic models. The reduced sensitivity of the equilibrated temperature gradient with strong thermal forcing is observed in the atmosphere and is the basis of baroclinic adjustment (Stone 1978), but this observational fact is explained from our quasi-linear model in a fundamentally different manner than in the manner usually associated with normal mode instability theory. In particular, the equilibration is not accomplished by a single, marginally unstable normal mode, it is accomplished by the cumulative effect of stochastically excited, transient eddies. Additionally, in contrast to baroclinic adjustment, the state of neutrality in the stochastic model is approached from the stable region, and the system is never unstable.

The curve associated with the quasi-linear model in Fig. 10 does not pass through the origin, having in this case an intercept at positive shear at $u_1 - u_2 = 0.5$, indicating that the stochastic model produces a baroclinic jet even when the thermal forcing relaxes the mean flow toward vanishing shear. Although the parameterization is not likely to hold for such weak shears, the result may be relevant to understanding the spontaneous formation of jets from stochastic excitation supplied by external mechanisms. A further interesting result is that the thermally forced state in the absence of eddies becomes linearly stable for $U_1^* - U_2^* < 17$ m s$^{-1}$, yet turbulent eddies still adjust the flow in the quasi- and nonlinear models. Lee and Held (1991) found that eddy kinetic energy can be maintained in a similar regime even when the state to which the flow is relaxed is stable. It is interesting that the quasi-linear model is consistent with this behavior without invoking disturbances that destabilize the flow.

The fact that our iteration scheme converges indicates that the quasi-linear equilibrium is a stable point of the implicitly nonlinear equations. This means that zonally symmetric perturbations to the quasi-linear equilibrated mean flow will tend to decay. Furthermore, when an external transport mechanism is introduced into the system, the shift toward a new configuration will be opposed by the eddies. This situation is consistent with the observed negative correlation between stationary and transient eddy heat fluxes (van Loon 1979; Stone and Miller 1980).

The decomposition of eddy kinetic energy into zonal wavenumbers for the quasi- and nonlinear equilibra-

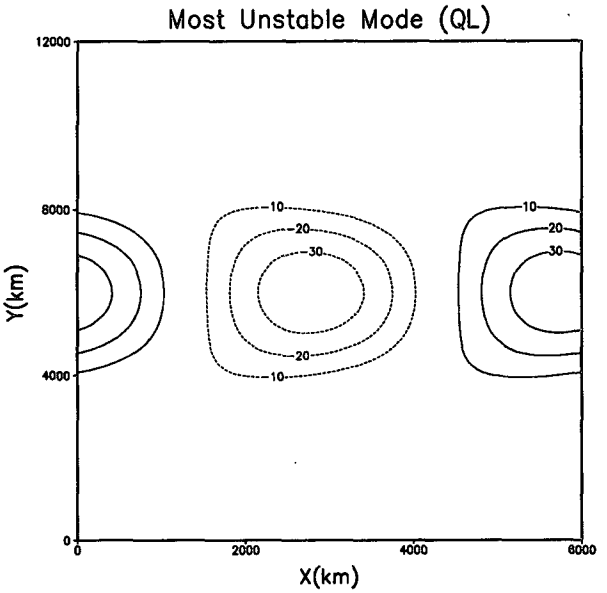


FIG. 16. Upper-layer streamfunction of the most unstable mode corresponding to the 1200-day average nonlinearly equilibrated flow. The zonal phase and amplitude are arbitrary. The similarity of this streamfunction to Figs. 14 and 15 suggests that this mode plays an important role in the response of both the nonlinear and quasi-linear equilibration.

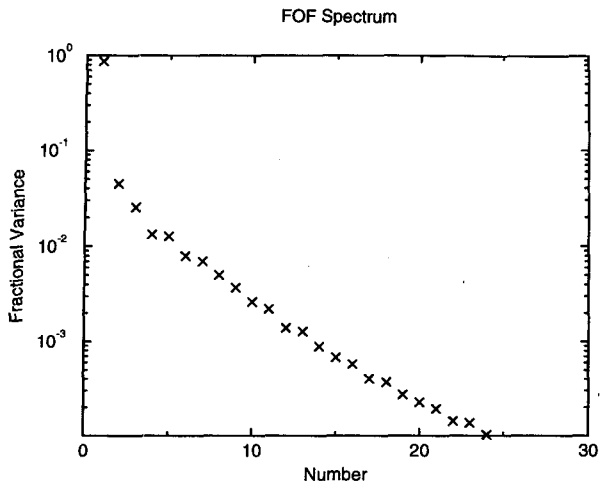


FIG. 17. Fractional variance excited by the FOFs in descending order for the quasi-linear equilibrium jet represented in Fig. 6. The magnitude of the variance excited by the first FOF exceeds by a factor of 6 that excited by the second.

tions is shown in Fig. 11. The result reveals that the energy spectra is sensitive to the magnitude of dissipation, which contrasts with the relatively smaller changes in the fluxes for the same parameter changes (Fig. 9). The reason for this contrast will be discussed in the next section.

To obtain the sources and sinks of eddy energy, we multiply (11) by $-\psi$ and (12) by $-\theta$ and integrate the sum of the resulting two equations over the entire region, invoking boundary conditions as needed. This gives an equation for the time rate of change of the eddy kinetic and potential energy E:

$$\frac{dE}{dt} = C(KM \rightarrow E) + C(PM \rightarrow E) + GE + DE + SE + DE_{EFF}, \quad (28)$$

where

$$C(KM \rightarrow E) = -U\overline{(\psi_x\psi_{yy} + \theta_x\theta_{yy})} - H\overline{(\psi_x\theta_{yy} + \theta_x\psi_{yy})} \quad (29)$$

$$C(PM \rightarrow E) = 2\lambda^2 H\overline{\psi_x\theta} \quad (30)$$

$$GE = -2\lambda^2 r_R\overline{\theta^2} \quad (31)$$

$$DE = -r_D\overline{(\psi_x^2 + \psi_y^2 + \theta_x^2 + \theta_x^2)} \quad (32)$$

$$SE = \overline{\psi\epsilon_\psi + \theta\epsilon_\theta} \quad (33)$$

$$DE_{EFF} = -r_E E \quad (34)$$

$$E = \frac{1}{2}\overline{((\psi_y)^2 + (\theta_y)^2 + (\psi_x)^2 + (\theta_x)^2)} + \lambda^2(\overline{\theta^2}). \quad (35)$$

The energy transfer among the eddies, mean flow, external dissipation, effective dissipation, and stochastic excitation are compiled in Table 3 for the first eight zonal wavenumbers. The overall balance is shown in Fig. 12a and indicates, as noted in the previous section, that eddies tend to extract energy from the mean available potential energy and inject energy into the mean kinetic energy. Moreover, the energy transfer implied by the forcing and dissipation associated with the parameterization balance each other, as is required for a consistent parameterization for the nonlinear terms. This balance was relatively easy to obtain by tuning the parameter $q$ in (19) and (20), which does little harm to the equilibrated state. There are a wide variety of consistencies and inconsistencies between the two models, but it is unclear which inconsistencies are in most need of improvement in future models.

The corresponding energy budget for the nonlinear model is given in Table 3b and illustrated in Fig. 12b. Except for the excessive frictional dissipation (DE), the quasi-linear energy cycle is remarkably consistent with the nonlinear solution. The quasi-linear model's enhancement of the frictional dissipation appears to be due to its overestimate of the eddy kinetic energy to which the dissipation is proportional. Importantly, the parameterized terms in the quasi-linear model can be strongly imbalanced and still give a realistic equilibrium. For instance, when $q$ is adjusted to inject 5 W m$^{-2}$, the effective dissipation that parameterizes the nonlinear scrambling damps just 4 W m$^{-2}$. Virtually the only difference between the respective equilibria is that the additional energy goes into barotropic eddy kinetic energy; the conversion terms and the eddy "generation" terms are hardly affected (and consequently, the equilibrated state is hardly affected). It is interesting that a reasonable equilibrated state can be

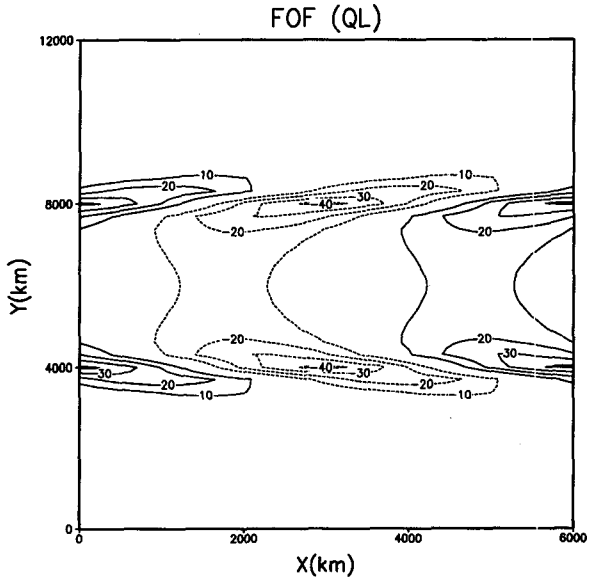


FIG. 18. Upper-layer streamfunction of the leading FOF for the quasi-linear equilibrium shown in Fig. 6. The figure shows only a portion of the channel corresponding to one zonal wavelength of wavenumber 5. The zonal phase and amplitude are arbitrary.

obtained even if the parameterization for the nonlinear terms do not consistently balance energy, suggesting that excitation of disturbances not significantly participating in wave–mean flow interactions can alter the energy balance without affecting the equilibrium state.

Quasigeostrophic nonlinear interactions also conserve enstrophy, but this constraint was not enforced by our methodology. The enstrophy budget equations can be derived in analogy with the energy budget equations by multiplying (11) by $\nabla^2\psi$ and (12) by $\nabla^2\theta - 2\lambda^2\theta$, and integrating the sum of the resulting equations over the domain. We make the following identifications:

$$C(BT \to Z) = U_{yy}(\overline{\psi_x\psi_{yy} + \theta_x\theta_{yy}}) + (H_{yy} - 2\lambda^2 H)(\overline{\psi_{yy}\theta_x + \psi_x\theta_{yy}}) \tag{36}$$

$$C(BC \to Z) = -(H_{yy} - 2\lambda^2 H)\overline{(2\lambda^2\psi_x\theta)} \tag{37}$$

$$GZ = -2\lambda^2 r_R\overline{(\theta_x^2 + \theta_y^2 + 2\lambda^2\theta^2)} \tag{38}$$

$$DZ = -r_D\overline{\{(\psi_{xx} + \psi_{yy})^2 + (\theta_{xx} + \theta_{yy})^2 - 2(\theta_{xx} + \theta_{yy})(\psi_{xx} + \psi_{yy}) + 2\lambda^2(\theta_x^2 + \theta_y^2 + \theta\psi_{xx} + \theta\psi_{yy})\}} \tag{39}$$

$$SZ = \overline{(\psi_{xx} + \psi_{yy})\epsilon_\psi + (\theta_{xx} + \theta_{yy} - 2\lambda^2\theta)\epsilon_\theta} \tag{40}$$

$$DZ_{EFF} = -r_E\overline{\{((\psi_{xx} + \psi_{yy})^2 + (\theta_{xx} + \theta_{yy})^2 + 2\lambda^2(\theta_x^2 + \theta_y^2))\}}. \tag{41}$$

The enstrophy budget for both the quasi-linear and nonlinear models is shown in Figs. 13a,b. There is a fairly large imbalance in the quasi-linear model between the conversions "SE" and "$D_{EFF}$." The other major difference is that the dissipation by the generation terms is underestimated by the quasi-linear model.

Interestingly, the sums of SZ + $DZ_{eff}$ and SE + $DE_{eff}$ for wavenumbers 5 and 6 are negative, indicating that the net explicit effect of the parameterization is to damp enstrophy and energy at these scales. This behavior is consistent with the nonlinear solution. While the net explicit effect of the parameterization for the nonlinear interactions is to damp these disturbances, stochastic injection is implicitly required to induce these disturbances to extract enstrophy and energy to maintain the equilibrated state.

## 6. Spatial structure of equilibrated eddies

We have so far considered the ensemble average statistics associated with the quasi-linear equilibrium without explicitly calculating the dominant spatial structures associated with these statistics. The following discussion focuses specifically on the quasi-linear equilibrium represented in Fig. 6, but applies generally to other cases. The first EOF (based on streamfunction) for both the fully nonlinear solution and the quasi-linear equilibrium are shown in Figs. 14 and 15, respectively. Both of these structures are similar to the most unstable mode of the linearized equations, shown in Fig. 16. The quasi-linear model itself does not require that the dominant EOF be similar to the most unstable mode, but in most cases they turn out to be similar.

Let us now consider the forcing structures that produce the maximum variance. This problem can be formulated in a way that is analogous to the way optimal disturbances for the initial value problem are derived (Farrell 1989). The optimal initial condition for the initial value problem can be formulated as the vector $\mathbf{e}$ giving the maximum norm response at time $\tau$ when impulsely introduced into a dynamical equation of the form

$$\frac{\partial\phi}{\partial t} = \mathbf{A}\phi + \mathbf{e}\delta(t) \tag{42}$$

$$\phi(0) = 0, \tag{43}$$

where $\mathbf{e}$ is normalized to $\mathbf{e}^H\mathbf{e} = 1$. It follows that the square Euclidean norm response at time $\tau$ is given by

$$\|\phi\|^2 = \mathbf{e}^H\{\exp(\mathbf{A}^H\tau)\exp(\mathbf{A}\tau)\}\mathbf{e}, \tag{44}$$

where $\|\phi\|$ is the $L_2$ norm of $\phi$. From the Rayleigh quotient theorem, the optimum form of $\mathbf{e}$ maximizing $\|\phi\|^2$ is the eigenvector of the matrix $(\exp(\mathbf{A}^H\tau)\exp(\mathbf{A}\tau))$ associated with the largest eigenvalue. The optimal forcing structures for the stochastic model, on the other hand, solves the problem of determining a vector $\mathbf{f}$ maximizing the time-averaged norm response under random excitation. These disturbances are called the forcing orthogonal functions. In this problem, the basic equation is one in which the delta function in (42) is replaced by a stochastic process and the optimizing time is dispensed with since only the ensemble average response is desired. For white noise forcing, the response can be shown to be

$$\langle\|\phi\|^2\rangle = \lim_{t\to\infty}\mathbf{e}^H\int_0^t \exp(\mathbf{A}^H(t-s))\times\exp(\mathbf{A}(t-s))ds\mathbf{e}. \tag{45}$$

Comparison with (44) shows that the matrix giving the FOF is related to the integral of the matrix giving the optimal impulse. It follows that the response of a stochastically excited system is determined not only by

the maximum transient amplification but also by the length of time transient disturbances persist.

The fractional variance associated with each FOF for zonal wavenumber 6 is shown in Fig. 17. We see that the first FOF excites a factor of 6 more variance than the second and a factor of 10 more than the third. The steepness of this FOF spectrum has the following important consequence: if each FOF were forced at comparable amplitudes, the first few FOFs would dominate the response at this wavenumber. Although the definition of an FOF implicitly includes the effective dissipation due to nonlinear scrambling, experimentation with Rayleigh friction and second-order diffusion, two significantly different but localized dissipations, were found to give essentially the same dominant FOF's. That effective dissipation is localized was independently suggested by the POP analysis of the nonlinearly equilibrated flow. It is plausible that the quasi-linear equilibrium is robust precisely because the leading FOFs are robust: the effect of dissipation on the subdominant FOFs is irrelevant because these FOF's have negligible impact on the eddy response.

The concept of FOF's clarifies why the eddy kinetic energy and the balance of stochastic energy injection and the dissipation can differ from that found in the nonlinear calculation. In particular, our approach of randomly exciting disturbances injects energy into disturbances that would presumably receive little energy from either nonlinear interactions or the mean flow. These disturbances are identified by the "weak" FOFs that negligibly interact with the basic state. As passive disturbances, they play little role in the equilibration even when they have large amplitudes, but they can affect the balance of terms in a budget equation.

It is well known that transient growth arises from the nonnormality of the underlying dynamical operator. Because the FOFs follow from integration of these transient disturbances, dominance of the leading FOF is also due to the nonnormality of the dynamical operator and the success of the quasi-linear model is in part a consequence of the high degree of nonnormality associated with the dynamical operator.

These results provide a way to understand the relation between optimal initial perturbations, usually studied in connection with the prediction of deterministic forecasts, and the FOFs that are the excitations more closely associated with the long-term climate. The connection is that the equilibrium climate results from the long-term average of a random series of transient developments excited by nonlinear eddy interactions.

The upper-layer structure of the first FOF for the quasi-linear equilibrium represented in Fig. 6 and shown in Fig. 18 exhibits the well-known phase tilt for developing disturbances in barotropic shear (it also tilts with respect to height so as to grow baroclinically). Although we have concentrated on the structure of disturbances in the upper-layer only, it should be recognized that similar structures exist in the lower layer. It should not be concluded that because the FOFs tilt against the horizontal and vertical shears that the equilibrated eddies will extract net energy from the barotropic and baroclinic components. The structure of the EOF determined from the quasi-linear model (Fig. 15) clearly indicates that the mean effect of the eddies is to transport momentum upgradient.

## 7. Discussion

The goal of this paper was to determine whether a model for quasigeostrophic turbulence in which nonlinear eddy terms are parameterized by stochastic excitation and Rayleigh friction can produce a realistic equilibrium jet structure. The parameterizations can be made to conserve the same quantities (on average) as the nonlinear terms they replace (Herring and Kraichnan 1972), but the usual techniques used to accommodate these constraints cannot easily be applied to cases involving baroclinic jets. DelSole (1996) has pointed out that principal oscillation pattern analysis can determine, in principle, the $n$th order Markov model with energy and enstrophy conserving parameterization for the eddy–eddy interactions, which yields the second-order (single time) moments of any realistic, turbulent equilibrium. Clearly then, a stochastic model can be contrived that exactly models the eddy fluxes. What is unclear is whether a stochastic model can be useful under simple parameter assumptions and in parameter regimes outside those for which the model has been tested.

In this study, the effective dissipation was assumed to be Rayleigh friction of equal magnitude in both layers and the stochastic excitation was assumed to be delta correlated between zonal and meridional wavenumbers, with meridional amplitudes weighted to produce a near Gaussian meridional structure. The resulting quasi-linear model was found to yield equilibrated heat fluxes, momentum fluxes, and mean states that were in remarkable agreement with the nonlinear model results over a wide range of parameter values despite energy and enstrophy imbalances associated with the parameterization for eddy–eddy interactions. Certain other choices of dissipation and stochastic excitation were also found to yield comparable agreement. The most obvious discrepancies between the quasi-linear and nonlinear solutions are the overestimate of eddy kinetic energy and the unbalanced enstrophy budget associated with the parameterization for eddy–eddy interactions, although these discrepancies appear to be correctable by restricting the excitation to a subset of disturbances that are dominantly active in producing wave–mean flow interaction.

The quasi-linear equilibration is consistent with baroclinic adjustment but the equilibration is accomplished in a fundamentally different manner than baroclinic adjustment as normally associated with linear, normal mode theory (Stone 1978; Stone and Branscome 1992). The conventional picture is based on the assumption that a rapid transition exists between con-

ditions in which the unstable eddy fluxes are relatively inefficient to conditions in which they are highly efficient (Stone 1978; Held 1978). The stochastic model, however, assumes disturbances have already been stabilized by the action of turbulent eddies even if the time mean flow happens to be linearly unstable. Nevertheless, the stochastic model does produce an enhanced response for small changes in mean temperature gradient (all other parameters held constant). This enhanced response can be understood in the stochastic model as a nonnormal resonance phenomenon in which the stochastic excitation excites a disturbance that is only slightly stable. However, the definition of neutrality in the stochastic model needs to include not only the effective dissipation due to turbulent eddies, but also the full three-dimensional structure of the mean flow. The latter component can introduce subtleties. For instance, the mean vertical shear slowly increases with thermal forcing in Fig. 10 because the barotropic component of the flow grows stronger and stabilizes the flow through the barotropic governor mechanism (James 1987), thereby allowing equilibration at larger shears.

The fact that the dissipation was chosen to be constant in this study should not be taken to suggest that the effective dissipation in the atmosphere *must* be constant. A physically motivated theory for the effective dissipation probably would have the damping increase with some measure of eddy activity.

The concept of FOFs can be used to clarify the quasi-linear dynamics in a variety of ways. The FOFs form an orthogonal set of spatial structures that maximize the linear, time-averaged (suitably defined) variance when the flow is stochastically forced with the structure of the FOFs (Farrell and Ioannou 1994). In many problems of interest, the spectra of the response is dominated by a small number of FOFs that are dominantly active in producing wave–mean flow interaction. In the particular case examined, the structure of the FOFs was not significantly altered when the effective dissipation was changed by an order of magnitude or when it was changed from Rayleigh friction to second-order diffusion. This explains how the quasi-linear equilibrium could remain the same for fundamentally different choices of effective dissipation. The remaining FOFs do not produce an appreciable interaction with the mean flow even when they are of large amplitude. This explains why the eddy kinetic energy of the quasi-linear equilibrium can be in error even when the equilibrated fluxes are accurate.

The concept of FOFs also clarifies certain limitations of the parameterization. In particular, the parameterization is not likely to work in a system characterized by a normal, linearized dynamical operator in which no transient growth is possible. As the degree of nonnormality decreases, the response spectrum of the FOFs typically becomes less peaked, and no single FOF can be guaranteed to dominate the response. Thus, the parameterization in this case would require more detailed specification of the excitation and dissipation to properly recover the response. In the limit of homogeneous turbulence in which the governing operator is normal, the details of the excitation and dissipation become paramount, as was found by Kraichnan (1959).

As an eddy transport parameterization, the approach outlined here has some advantages compared to other parameterizations. One advantage is that the heat and momentum fluxes are consistently derived from the complete dynamical operator associated with the linearized equations rather than from a single normal mode. Moreover, the precise statistical nature of the nonlinear interactions are directly specified allowing a clearer interpretation of the eddy dynamics. As a climate model, the quasi-linear model suffers from severe deficiencies compared to a general circulation model. In particular, there is no a priori theory for choosing the effective dissipation and stochastic excitation. The robustness of the quasi-linear equilibrium with respect to parameter changes suggests that the model can still be useful in cases in which the parameters are only approximately known. In such cases, the quasi-linear model can be a powerful tool for addressing climate equilibration problems since it can be solved much faster than the nonlinear model.

We stress that the quasi-linear approach developed here is not restricted to the two-layer quasigeostrophic model and should, we believe, apply to virtually any nonlinear turbulent system characterized by a highly nonnormal linearized dynamical operator. In studies not reported here, we found that the quasi-linear equilibration of a barotropically unstable mean flow [achieved by setting $b = 600$ km in (21)] gave a remarkably similar jet to that of the corresponding nonlinear solution for the same effective dissipation and stochastic excitation used in the baroclinic case. The approach outlined in this study therefore appears to offer a general and fundamentally new way of understanding the role of transient eddies in climate.

*Acknowledgments.* The authors would like to thank Peter Stone and Petros Ioannou for helpful discussions regarding this work. Comments from an anonymous reviewer were especially valuable. Part of this work is based on T. DelSole's doctoral thesis while supported by a NASA Global Change Graduate Fellowship. Much of this work was completed while T. DelSole was supported by a U.S. Department of Energy Global Change Distinguished Postdoctoral Fellowship, administered by Oak Ridge Institute for Science and Education, and hosted by the National Aeronautics and Space Administration/Goddard Space Flight Center. Brian Farrell was partially funded by the U.S. Department of Energy's (DOE) National Institute for Global Environmental Change (NIGEC) through the NIGEC Northeast Regional Center at Harvard University (DOE Cooperative Agreement No. DE-FC03-90ER61010). Financial support does

not constitute an endorsement by DOE of the views expressed in this article. B. Farrell was also supported by NSF Grant ATM-9216813.

APPENDIX A

## Calculation of Covariances

Suppose the linear stochastically forced equations to be solved are written in matrix form as

$$\phi_t = \mathbf{A}\phi + \zeta(t). \tag{A1}$$

Standard techniques give the solution

$$\phi(t) = \int_0^t \exp(\mathbf{A}(t-s))\zeta(s)ds. \tag{A2}$$

Assuming the excitation $\zeta$ is white noise such that

$$\langle \zeta(s)\zeta^{\mathrm{H}}(s')\rangle = \mathbf{Q}\delta(s-s'), \tag{A3}$$

the covariance matrix is found to be

$$\mathbf{C}(t) = \langle \phi(t)\phi^{\mathrm{H}}(t)\rangle = \int_0^t \exp(\mathbf{A}(t-s))\mathbf{Q} \times \exp(\mathbf{A}^{\mathrm{H}}(t-s))ds. \tag{A4}$$

Differentiating this with respect to time yields

$$\mathbf{0} = \mathbf{AC} + \mathbf{CA}^{\mathrm{H}} + \mathbf{Q}, \tag{A5}$$

where $d\mathbf{C}/dt = 0$ due to stationarity. This equation is called the Lyapunov equation and standard matrix techniques can be applied to solve this equation for $\mathbf{C}$ (Gardiner 1990). The energy of the response is $-\frac{1}{2}\phi^{\mathrm{H}}\mathbf{B}\phi$, where $\mathbf{B}$ is the Hermitian potential vorticity operator such that $\mathbf{q} = \mathbf{B}\phi$. The energy tendency is found by evaluating $\phi^{\mathrm{H}}\mathbf{B}^{\mathrm{H}}(\mathrm{A1}) + (\mathrm{A1})^{\mathrm{H}}\mathbf{B}\phi$:

$$-\frac{1}{2}(\phi^{\mathrm{H}}\mathbf{B}\phi)_t = -\frac{1}{2}\,\mathrm{Trace}(\mathbf{B}(\mathbf{AC} + \mathbf{CA}^{\mathrm{H}} + \mathbf{Q})).$$

The term $-1/2\ \mathrm{Trace}(\mathbf{BQ})$ represents the total energy injection by stochastic forcing and is positive.

APPENDIX B

## Spectral Solution

The solution of the stochastically forced linear equations is most easily obtained using a spectral technique in which the mean velocities are represented as

$$\mathrm{U}(y) = -\Psi_y = \sum_m \mathrm{U}_m \sin(\pi my/L_y)$$

$$\mathrm{H}(y) = -\Theta_y = \sum_m \mathrm{H}_m \sin(\pi my/L_y)$$

$$\mathrm{H}^*(y) = -\Theta_y^* = \sum_m \mathrm{H}_m^* \sin(\pi my/L_y) \tag{B1}$$

and the perturbation quantities as

$$\begin{pmatrix}\psi(x,y,t)\\ \theta(x,y,t)\end{pmatrix} = \mathrm{Re}\left(\sum_l \sum_k \begin{pmatrix}\psi_{k,l}(t)\\ \theta_{k,l}(t)\end{pmatrix} \sin(\pi ly/L_y)e^{ikx}\right). \tag{B2}$$

[See Cehelsky and Tung (1987) for justification of this orthogonal basis set.] The ensemble average covariances of the stochastically forced linear equations are substituted in (9) and (10). For a fixed zonal wavenumber and after eliminating $w$, the mean equations (9) and (10) can be written as

$$\frac{d\mathrm{U}_m}{dt} = D_m - (\mathrm{U}_m - \mathrm{H}_m)\mathrm{r_D} \tag{B3}$$

$$\frac{d\mathrm{H}_m}{dt} = \mathrm{E_m} - \frac{(\mathrm{H}_m - \mathrm{U}_m)m^2\mathrm{r_D}}{m^2 + 2\lambda^2} + \frac{(\mathrm{H}_m^* - \mathrm{H}_m)2\lambda^2\mathrm{r_R}}{m^2 + 2\lambda^2}, \tag{B4}$$

where

$$D_m = \sum_{j,l} \mathrm{Im}[\langle \psi_j\psi_l^* + \theta_j\theta_l^*\rangle]kl^2d_{jlm} \tag{B5}$$

$$\mathrm{E}_m = \sum_{j,l} k\,\mathrm{Im}[\langle \psi_j\theta_l^*\rangle] \times \frac{(l^2 - j^2 + 2\lambda^2)((l^2 + j^2)d_{jlm} - 2jle_{jlm})}{m^2 + 2\lambda^2} \tag{B6}$$

$$d_{jlm} = \frac{-8jlm}{\pi(j^2 - (l^2 + m^2))(j^2 - (l^2 - m^2))}\,\delta_{j+l+m=\mathrm{odd}} \tag{B7}$$

$$e_{jlm} = \frac{4m(m^2 - l^2 + j^2)}{\pi(j^2 - (l^2 + m^2))(j^2 - (l^2 - m^2))}\,\delta_{j+l+m=\mathrm{odd}}, \tag{B8}$$

in which $\delta_L$ is 1 if the statement $L$ is true and is 0 if $L$ is false.

APPENDIX C

## Semi-Implicit Integration

We wish to solve the set of equations (A3) and (A4). Suppose these equations are written in the form

$$\frac{d\mathbf{M}}{dt} = \mathbf{G}[\mathbf{M}]. \tag{C1}$$

This is generally a nonlinear equation because the velocities, denoted by $\mathbf{M}$, depend nonlinearly on $\mathbf{C}$, the covariance matrix. Because $d\mathbf{M}/dt$ varies by orders of magnitude for different waves, the set of equations (C1) are "stiff" and are difficult to solve with explicit integration techniques such as Runge–Kutta (Press et al. 1992). To overcome this difficulty, we have developed the following implicit iterative method. Let $h$ be

the time step and $\mathbf{M}^n$ refer to the value of $\mathbf{M}$ at the $n$th time step. Implicit differencing yields

$$\mathbf{M}^{n+1} = \mathbf{M}^n + h\mathbf{G}[\mathbf{M}^{n+1}]. \quad \text{(C2)}$$

Since $\mathbf{B}$ is a highly nonlinear function of $\mathbf{M}^{n+1}$ and cannot be inverted, we proceed by linearizing the equation

$$\mathbf{M}^{n+1} = \mathbf{M}^n + h\left\{\mathbf{B}[\mathbf{M}^n] + \frac{\partial \mathbf{G}}{\partial \mathbf{M}}(\mathbf{M}^{n+1} - \mathbf{M}^n)\right\}. \quad \text{(C3)}$$

Here, $\partial\mathbf{G}/\partial\mathbf{M}$ is the Jacobian matrix of the partial derivatives. The Jacobian matrix can be obtained directly from the covariance matrix. By rearranging (C3), we obtain an equation suitable for iteration:

$$\mathbf{M}^{n+1} = \mathbf{M}^n + h\left(1 - h\frac{\partial \mathbf{G}}{\partial \mathbf{G}}\right)^{-1}\mathbf{G}[\mathbf{M}^n]. \quad \text{(C4)}$$

Although (C4) requires inverting a matrix at each iteration, the solution is now stable for most values of the time step $h$. Unfortunately, the covariance matrix cannot be evaluated for unstable flows, so the timestep must be sufficiently small to avoid inadvertently crossing the stability boundary during the iteration.

Evaluating the Jacobian matrix requires finding the derivative of the covariance matrix with respect to the velocity. The result is a third-order tensor that requires order $N^4$ calculations for its evaluation. However, Farrell and Ioannou (1993) show that the covariance matrix solves a Lyapunov equation, therefore the derivatives of the covariance matrix are found by differentiating the Lyapunov equation with respect to velocities. This differentiation yields another Lyapunov equation that can be solved by standard methods.

## REFERENCES


Arakawa, A., 1966: Computational design for long-term numerical integration of the equations of fluid motion. *J. Comput. Phys.*, **1,** 119–143.

Branscome, L. E., 1983: A parameterization of transient eddy heat flux on a beta-plane. *J. Atmos. Sci.*, **40,** 2508–2521.

Cehelsky, P., and K. K. Tung, 1987: Theories of multiple equilibria and weather regimes—A critical reexamination. Part II: Baroclinic two-layer models. *J. Atmos. Sci.*, **44,** 3283–3303.

Charney, J. G., 1947: The dynamics of long waves in a baroclinic westerly current. *J. Meteor.*, **4,** 135–163.

DelSole, T., 1996: Can quasigeostrophic turbulence be modeled stochastically? *J. Atmos. Sci.*, **53,** 1617–1633.

——, and B. F. Farrell, 1995: A stochastically excited linear system as a model for quasigeostrophic turbulence: Analytic results for one- and two-layer fluids. *J. Atmos. Sci.*, **52,** 2531–2547.

Durran, D. R., 1991: The third-order Adams–Bashforth method: An attractive alternative to leapfrog time differencing. *Mon. Wea. Rev.*, **119,** 702–720.

Eady, E. T., 1949: Long waves and cyclone waves. *Tellus*, **1,** 35–52.

Farrell, B. F., 1982: The initial growth of disturbances in a baroclinic flow. *J. Atmos. Sci.*, **39,** 1663–1686.

——, 1984: Modal and nonmodal baroclinic waves. *J. Atmos. Sci.*, **41,** 668–673.

——, 1985: Transient growth of damped baroclinic waves. *J. Atmos. Sci.*, **42,** 2718–2727.

——, 1989: Optimal excitation of baroclinic waves. *J. Atmos. Sci.*, **46,** 1193–1206.

——, and P. J. Ioannou, 1993: Stochastic dynamics of baroclinic waves. *J. Atmos. Sci.*, **50,** 4044–4057.

——, and ——, 1994: A theory for the statistical equilibrium energy and heat flux produced by transient baroclinic waves. *J. Atmos. Sci.*, **51,** 2685–2698.

——, and ——, 1995: Stochastic dynamics of the midlatitude atmospheric jet. *J. Atmos. Sci.*, **52,** 1642–1656.

Gardiner, C. W., 1990: *Handbook of Stochastic Methods.* 2d ed. Springer-Verlag, 442 pp.

Gutowski, W. J., 1985: A simple model for the interaction between vertical eddy heat fluxes and static stability. *J. Atmos. Sci.*, **42,** 346–358.

Held, I. M., 1978: The vertical scale of an unstable baroclinic wave and its importance for eddy heat flux parameterizations. *J. Atmos. Sci.*, **35,** 572–576.

Herring, J. R., and R. H. Kraichnan, 1972: Comparison of some approximations for isotropic turbulence. *Statistical Models and Turbulence.* M. Rosenblatt and C. Van Atta, Eds., Springer-Verlag, 148–194.

James, I. N., 1987: Suppression of baroclinic instability in horizontally sheared flows. *J. Atmos. Sci.*, **44,** 3710–3720.

Kraichnan, R. H., 1959: The structure of isotropic turbulence at very high Reynolds numbers. *J. Fluid Mech.*, **5,** 497–543.

Lee, S., and I. M. Held, 1991: Subcritical instability and hysteresis in a two-layer model. *J. Atmos. Sci.*, **48,** 1071–1077.

Lindzen, R. S., 1993: Baroclinic neutrality and the tropopause. *J. Atmos. Sci.*, **50,** 1148–1151.

——, and B. Farrell, 1980: The role of polar regions in global climate, and a new parameterization of global heat transport. *Mon. Wea. Rev.*, **108,** 2064–2079.

Penland, C., 1989: Random forcing and forecasting using principal oscillation pattern analysis. *Mon. Wea. Rev.*, **117,** 2165–2185.

Press, W. H., S. A. Teukolsky, W. T. Vetterling, and B. P. Flannery, 1992: *Numerical Recipes.* Cambridge University Press, 963.

Stone, P. H., 1978: Baroclinic adjustment. *J. Atmos. Sci.*, **35,** 561–571.

——, and D. A. Miller, 1980: Empirical relations between seasonal changes in meridional temperature gradients and meridional fluxes of heat. *J. Atmos. Sci.*, **37,** 1708–1721.

——, and L. Branscome, 1992: Diabatically forced, nearly inviscid eddy regimes. *J. Atmos. Sci.*, **49,** 355–367.

van Loon, H., 1979: The association between latitudinal temperature gradient and eddy transport. Part I: Transport of sensible heat in winter. *Mon. Wea. Rev.*, **107,** 525–534.

von Storch, H., G. Burger, R. Schnur, and J.-S. von Storch, 1995: Principal oscillation patterns: A review. *J. Climate*, **8,** 377–400.